Capillary force in adhesive contact between hydrogel microspheres

Lidong Liu and Kuo-Kang Liu* *I.K.Liu@warwick.ac.uk*

School of Engineering, University of Warwick, Library Road, Coventry, CV4 7AL, UK

Author for correspondence:

Kuo-Kang Liu

School of Engineering

University of Warwick

Coventry CV4 7AL

Tel: + 44 (0)24 76574348

Fax: +44 (0)24 76418922

Email:

Graphical abstract

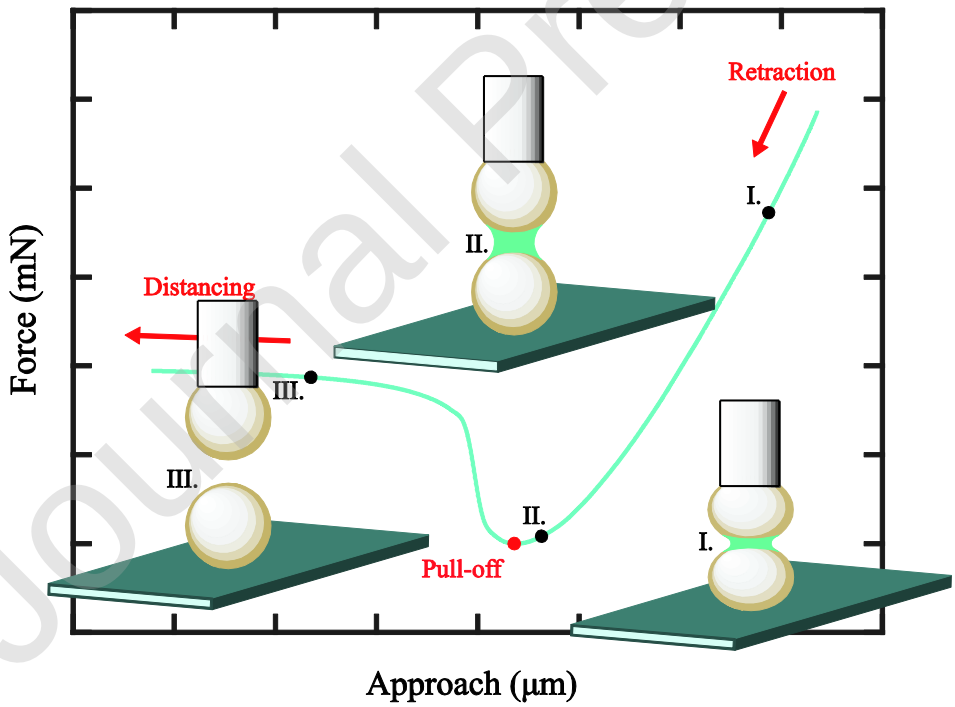

Pull-off testing for measuring the capillary force between particles.

ABSTRACT: The paper reports an experimental study of the adhesive contact between liquid-bridged hydrogel microparticles. A novel nanomechanical tester has been developed to measure both the force-approach curves at sub-micro resolutions as well as the side-view images between two agarose spheres during pull-off. Meanwhile, the JKR theory has been extended to quantify the work of adhesion at the solid-liquid-vapor interface and Young's modulus of the particles based on the measured parameters. Our research findings show the work of adhesion is independent of the separation speed and, by contrast, Young's modulus exhibits a linear increase. Our study also demonstrates that JKR reconciles with the generalized Hertz theory, which takes capillary force into account for soft microspheres in a relationship that the work of adhesion is equal to twice the surface tension of water. These new findings are essential for developing techniques to quantitatively characterize capillary adhesion of soft particulate materials and potentially to improve the material performance in their applications.

KEYWORDS: Adhesion; Soft Matter; Contact Mechanics; Capillary Force; Interfacial Properties; Viscoelasticity.

1. Introduction

When the liquid fills the narrow gap between two solid surfaces, it forms a meniscus leading to an attraction called capillary force[1]. It is a ubiquitous phenomenon in the particulate materials ranging from granular powder[2,3] to biological cells[4,5]. Recently hydrogel particles have been widely used in food, pharmaceutical and biomaterial industries[6]. Since these particles typically contain a high percentage of

water, the capillary force plays an important in their adhesive contact[7,8]. The quantitative characterization of capillary adhesion is therefore essential for better understanding their interparticle interactions and improving mechanical and interfacial properties in their applications.

Classical contact mechanics and adhesion theories such as Johnson-Kendall-Roberts (JKR)[9] and Derjaguin-Muller-Toporov (DMT)[10] provide a fundamental understanding of the contact and adhesion between surfaces. Despite the fact that most theories are developed under the assumption of solid-solid contact, previous studies[11,12] showed that they could be potentially applied to complex contact situations such as a solid-liquid-vapor interface. Recently, extended contact theories for the complex contact are in demand, partly because of increasing interest in soft polymeric microparticles[13,14] and biological cells[15], which are characterized by small dimensions and relatively low Young's moduli. Recent theoretical and computational studies shed light on how capillary force influences the adhesive contact between two rigid particles[16] as well as a rigid particle to a soft substrate[17,18].

Despite theoretical studies extensively reported, experimental measurements of capillary adhesion between hydrogel particles remain challenging because interparticle forces typically range from few nanonewtons (nN) to hundreds of micronewtons (μN) depending on the particle sizes. Ultrasensitive instruments for force-displacement measurement are therefore essential for experimental investigations of the capillary-dominant adhesive contact between two hydrogel microspheres. AFM has long been recognized as a powerful technique to study capillary adhesion thanks to its capability in measuring force-displacement on nanoscale objects or surfaces. Extensive AFM-based investigations in various effects, such as hydrophilicity[19], relative

humidity[20], ionic diffusion[21] and surface roughness[22], influencing on the capillary forces between nanoparticle and solid surface have been reported. Notwithstanding its superiority in force and displacement sensing, the challenge remains for using AFM to directly measure capillary adhesion between soft microparticles because accurate alignment between the particles is difficult to achieve. Alternatively, Surface-Force-Apparatus (SFA) has been used to study capillary forces between interacting surfaces across fluid media[23]. SFA is ideally suited for rigid surface-surface interactions, longer-range forces and surfaces interactions with long relaxation times such as adhesive contact between high-viscosity materials. However, SFA-based measurement for capillary adhesion between soft particles is not feasible due to the limitation in its instrumental setup. There is therefore a need for new advancement in experimental technique to measure the capillary influence in adhesion between soft particles. In this study, we developed a novel nanomechanical tester to measure the pull-off force and side-view profiles between two hydrogel microspheres during separation. Contact theories such as JKR and generalized Hertzian theories have applied to interpret quantitatively the capillary-dominant adhesion. The comparison between the experimental measurements and theoretical predictions facilitates the determination of the work of adhesion and Young's modulus of the particles.

2. Experimental Section

2.1. Fabrication of Hydrogel Microparticles

Hydro-gel spheres were made of 1.5 weight % agarose (Sigma Life Science, low gelling temperature agarose, A9414). The agarose powder was suspended in deionized water at 20^{o}C and heated to 85^{o}C in a water bath (Grant Instruments Ltd, JB Nova Unstirred JBN12) to allow the powder to fully dissolve. The solution was then dispersed through a spray nozzle into vegetable oil (Flora, pure sunflower oil, 392803) to produce

micron-size particles that are essentially spherical due to surface tension. Depending on the spray velocity and nozzle dimension, the range of particle sizes lies between 200 to 1000 μm in diameter.

2.2. Preparation of Hydrogel Disk

A disk-shaped sample of agarose gel was prepared for the indentation test to independently characterize Young's modulus of the gel (see Section 2.4). Fully-dissolved agarose solution at 85°C was poured into a petri dish of 5 cm in diameter and 2 cm in thickness, respectively. The petri dish was then cooled in a humidity-controlled chamber (ibidi GmbH, Gas Mixer M-323) with 80% relative humidity under room temperature (20 °C) until the solution was solidified to form the gel sample.

2.3. Capillary Adhesion Measurements

An ultra-sensitive instrument was developed and constructed to directly measure the separation force-displacement curves between two liquid-bridged particles (Figure 1). One agarose sphere was selected and attached on the flat surface of a force transducer probe (Aurora Scientific, 406A) with a force resolution of 10 nN, which was driven by a micro-stepper stage with a discrete displacement resolution of 10 nm in *Z*-direction (Newport, UTS 100CC with ESP301 Motion Controller). The second sphere was firmly glued on a flat glass substrate to prevent it from sliding throughout the whole contact process. An *X*-*Y* motorized stage (Prior Scientific, H117P1T4) was used to ensure the two poles aligned axially (100nm resolution in both *X* and *Y* directions). The top sphere was lowered at a constant speed (20μm/s) by the *Z*-stage till a ca. 25 μm approach (the compressive displacement at the pole of deformed spheres) was reached to form a finite solid-solid contact. After 3 seconds contact time, the actuator was then retracted at the same speed to shrink the contact area till 'pull-off'. The force-approach curves were measured and recorded using a data acquisition system (National Instruments, SCC-

68). A grayscale CCD (Sony, XC-ST50ce) with a long focal lens (Edmund Industrial Optics, VZM 450) was used to capture the simultaneous side-view profiles (see Figure 2(a)). The whole measurement instrument was supported by an anti-vibration table (Wentworth Laboratories Ltd, ATV 702),

Figure 1.

Figure 2.

Agarose gel has been well recognized as homogeneous and isotropic material which contains a high percentage of water (ca. 98.5% W/W for the current spheres). When the hydrogel spheres were brought into intimate contact in air, a compression developed at the contact circle deformed the spheres and raised the elastic energy stored in the viscoelastic medium of agarose. The compression also squeezed a minute amount of water from the saturated spongy materials, leading to a meniscus at the annulus around the contact circle.

Measurements were repeated for spheres with a range of dimensions as well as a range of loading-unloading speeds (10–30 μm/s). At least three replications of the force-approach curve have been measured for each dimension at each separation speed. During the entire separation period, side-view images of the two spheres were acquired dynamically by the CCD camera. The captured images were then processed by MATLAB (MathWorks, R2017a) using an edge detection algorithm to determine two principal radii r_1 and r_2 of the meniscus (see Figure 2(b)).

The acquired images (see Figure 3) show the liquid re-absorption process is swift and the liquid re-absorbed fully within *ca* 0.166s after the capillary bridge was broken. The sphere volumes were measured based on the captured images before and after each group of experiments performed; the volume change during the measurement period due to liquid vaporization was found to be negligible. During the entire measurement

periods, an illuminator was used to illuminate the two spheres for enhancing the acquired image qualities.

Figure 3.

2.4. Indentation Testing

For an independent characterization of the agarose's elasticity, an alternative setup was constructed based on the same force-displacement sensing platform mentioned above to perform indentation testing of the materials. A PMMA (polymethyl methacrylate) sphere with 800 μm in diameter was installed on the tip of the force sensor to serve as a spherical indenter. Young's modulus of the PMMA was selected to range from 1800 to 3100 MPa, that is, about 10000 times higher than those of agarose gel, to ensure the deformation of the indenter negligible during indentation. The PMMA bead was then lowered at a constant speed (20 μm/s) to indent the disk-shaped gel sample up to 30 μm (see Figure 4). The force-indentation depth curves were measured and used to estimate the values of Young's modulus for cross-validation of those of the agarose particles measured by the aforementioned pull-off test.

Figure 4.

3. Theoretical Basis

3.1. Contact Mechanics and Adhesion

On the theoretical front, the classic Hertz contact theory describes the non-adhesive contact between two deformable elastic spheres[24]. When a compressive contact normal load P is applied to two elastic spheres along the aligned axes, it creates a circular radius a and an approach δ, Hertz contact theory requires

$$\delta_{Hertz} = \frac{{a_{Hertz}}^2}{R}, \quad (1)$$

$$P = \frac{4E^* {a_{Hertz}}^3}{3R}, \tag{2}$$

where E^* is the reduced Young's modulus, and R is the effective radius, respectively, defined by:

$$\frac{1}{E^*} = \frac{1-\nu_1^2}{E_1} + \frac{1-\nu_2^2}{E_2}, \tag{3}$$

and

$$R = \frac{R_1 R_2}{R_1 + R_2}, \tag{4}$$

where ν is Poisson's ratio and E is Young's modulus; the subscripts denote spheres 1 and 2.

Equation (2) can be rewritten into a simpler form

$${a_{Hertz}}^3 = \frac{RP}{K}, \tag{5}$$

and $K = {4E^*}/{3}$.

In JKR theory[9], a work of adhesion $\Delta\gamma$, which is defined as a reversible thermodynamic work per unit area that is needed to separate an interface from the equilibrium state of two phases to a separation distance of infinity, is incorporated into the Hertz theory, yielding a new contact radius and a new approach of

$$a_{JKR} = \left(\frac{R}{K}P_1\right)^{1/3} = \left[\frac{R}{K}\left(P + 3\Delta\gamma\pi R + \sqrt{6\Delta\gamma\pi RP + (3\Delta\gamma\pi R)^2}\right)\right]^{1/3}, \tag{6}$$

$$\delta_{JKR} = \frac{{a_{JKR}}^2}{R} - \sqrt{\frac{8\Delta\gamma\pi a_{JKR}}{3K}}. \tag{7}$$

The JKR analysis takes into account the adhesion force of the solids by including the surface energy. Young-Dupré[25] requires $\Delta\gamma = \gamma_1 + \gamma_2 - \gamma_{12}$, γ represents the interfacial surface energy, where the subscripts denote surface 1 and 2 (interfacial energy between solid and vapor), and the interface 12. Consequently, the apparent Hertz

load P_1 is greater than the applied contact normal load P, as described by the equation (6).

Removal of the applied normal load (i.e., $P = 0$) reduces the contact radius to a_0 given by

$$a_0 = \left(\frac{6\pi\Delta\gamma R^2}{K}\right)^{1/3}. \tag{8}$$

An extensive form of equation (5) for JKR can be given as

$$a_{jkr}^3 - \left(a_0 a_{jkr}\right)^{3/2} = \frac{PR}{K}. \tag{9}$$

Detailed descriptions of the DMT theory are given elsewhere[10]. Tabor[26] and Maugis[12] discussed the difference between these two limiting solutions. They proposed a transition from the DMT to JKR limit which can be governed by a dimensionless characteristic parameter, representing the ratio between the height of the neck around the contact zone and the equilibrium separation distance between the atoms at the interface. This parameter is well known as the Tabor parameter (see below).

If a liquid droplet is trapped at the contact interface (again, see Figure 2(b)), the adhesion force F_{adh} which is attributed to the capillary bridge is given by[27]

$$F_{adh} \cong F_{cap}(\Delta p), \tag{10}$$

where $F_{cap}(\Delta p)$ is the capillary force due to the Laplace pressure[28] within the meniscus given by:

$$\Delta p = \gamma_{LV}\left(\frac{1}{r_1} + \frac{1}{r_2}\right) = \frac{\gamma_{LV}}{r_m}, \tag{11}$$

where r_1 and r_2 are the two principal radii to describe the curvatures of the meniscus, r_m is the harmonic mean radius, and the γ_{LV} is the liquid/vapor surface tension. Note that r_m is negative due to $\Delta p < 0$.

Fogden and White[29] proposed a generalized Hertz theory which accounts for the Laplace pressure. A constant k is introduced

$$k = \frac{3\pi^{1/2}}{2^{3/2}} \frac{\left(-r_m - \frac{1}{2}D_0\right)^{3/2} K}{2\gamma_{LV} R^{1/2}} \left(1 + \frac{D_0}{2r_m}\right)^{-1}. \quad (12)$$

The authors also considered the possibility that a repulsive force between the two surfaces may prevent them from coming into molecular contact, and thus D_0 is the minimum separation distance between the two surfaces and the finite contact radius a_0 generated from the interfacial adhesion can be rewritten as:

$$a_0 = \left(12\pi\gamma_{LV}\left(1 + \frac{D_0}{2r_m}\right)R^2/K\right)^{1/3}. \quad (13)$$

According to their theory, a small k represents relatively large and soft spheres with vapor pressure close to the values marking the onset of capillary condensation. For such a system, a generalized Hertzian contact radius-load relationship may be expressed,

$$a^3 - (a_0 a)^{3/2} = \frac{PR}{K}. \quad (14)$$

Intriguingly, the mathematical similarity between equations (14) and (9) alludes to that the generalized Hertzian and JKR may possess a similar origin in their adhesion. However, the two theories present different formulations in terms of a_0, owing to their distinctive adhesion sources.

For a system with a relatively large radius of the meniscus, i.e. $D_0 \ll -2r_m$, the solid-solid repulsive effect becomes insignificant[27] and the equation (13) can then be simplified as

$$a_0 = \left(\frac{12\pi\gamma_{LV}R^2}{K}\right)^{1/3}. \quad (15)$$

Comparing equation (8) with equation (15), the two theories may be reconciled by the following relationship between the work of adhesion and the surface tension:

$$\Delta\gamma = 2\gamma_{LV}. \tag{16}$$

Prior to Fogden and White derived the system constant k, Tabor[26] has introduced a similar non-dimensional parameter μ_T, which is well known as the Tabor parameter to describe the JKR-DMT transition for solid-to-solid elastic adhesion. For JKR solution, both compressive and tensile stress act in the area of contact, and no force occurs outside. On the contrary, for DMT solution, the repulsive pressure only acts in the area of contact, and adhesive force simply adds to the Hertz problem outside the contact area. Later Xu *et al.* [30] proposed a modified Tabor parameter for the contact in the presence of capillary condensation as

$$\mu_T^c = \left(\frac{2R\Delta\gamma^2}{9K^2 r_m^3}\right)^{1/3}. \tag{17}$$

As mentioned above, for a system with relatively large radii of the meniscus, $D_0 \ll -2r_m$, then equation (12) reduces to another form where can be seen a strong correspondence with equation (17):

$$\mu_T^c = \left(\frac{\pi}{4}k^{-2}\right)^{1/3}. \tag{18}$$

Essentially, the Fogden and White's system constant is an alternative mathematical expression of the modified Tabor parameter for the adhesive contact in the presence of meniscus condensation. To summarize, the JKR model is valid for a relatively soft and large system roughly $\mu_T^c > 2$, which is corresponding to $k < 0.3$ (Cf. equation (18)), and the DMT model is valid for a relatively small and rigid system, $\mu_T^c < 0.1$[31].

3.2. Viscoelastic Model

A theoretical model to describe viscoelastic adhesive contact[32] is applied to interpret the rate-dependent elastic modulus of the agarose spheres. Based on the theory, substituting the elastic modulus-approach convolution into Hertz contact theory will give a force-approach relationship in the time domain[33] as

$$P(t) = \frac{4\sqrt{R}}{3(1-\nu^2)} E(t) * [\delta(t)]^{3/2} \tag{19}$$

where $E(t)$ is the relaxed modulus of the spheres.

$$E(t) * [\delta(t)]^{3/2} = \int_{\xi=0^-}^{t} E(t-\xi) \frac{d}{d\xi} [\delta(\xi)]^{3/2} d\xi \tag{20}$$

Since the two spheres approached and separated at a constant speed in the experimental measurements, the approach can be expressed as:

$$\delta = Vt \tag{21}$$

where V denotes the constant speed.

Equation (19) is transformed into the Laplace domain to describe the viscoelastic responses:

$$\overline{P(s)} = \frac{4\sqrt{R}}{3(1-\nu^2)} \overline{E(s)} \cdot \overline{\delta(s)^{3/2}} \tag{22}$$

where $\overline{P(s)} = \int_0^\infty P(t) e^{-st} dt$, $\overline{E(s)} = \int_0^\infty E(t) e^{-st} dt$, and $\overline{\delta(s)^{3/2}} = \int_0^\infty [\delta(t)]^{3/2} e^{-st}\, dt$

Substitution of equation (21) with equation (22) yields:

$$\overline{P(s)} = \frac{4\sqrt{R} V^{3/2}}{3(1-\nu^2)} \overline{E(s)} \cdot \frac{\Gamma(5/2)}{s^{5/2}} \tag{23}$$

where Γ is a gamma function.

For modelling viscoelastic behaviors of hydrogel material, Voigt model, which consists of a Newtonian dashpot and linear elastic spring connected in parallel (Figure 1A. in Appendix) is applied. The constitutive equation to describe the stress-strain relationship of a homogenous hydrogel can be expressed as[34]

$$\sigma = E_0 \varepsilon + \mu \frac{d\varepsilon}{dt} = E(t)\varepsilon \tag{24}$$

where σ and ε are stress and strain, respectively, E_0 denotes elastic modulus in the steady-state (or Young's modulus) and μ is the viscosity coefficient.

Equation (24) can be transformed into its Laplace domain as:

$$\frac{\overline{\sigma(s)}}{\overline{\varepsilon(s)}} = (E_0 + \mu s) \tag{25}$$

where $\overline{\sigma(s)} = \int_0^\infty \sigma(t)e^{-st}dt$, $\overline{\varepsilon(s)} = \int_0^\infty \varepsilon(t)e^{-st}dt$.

According to the correspondence principle[35], the general elastic and viscoelastic solutions can be combined into the Laplace domain to obtain an equation describing Young's modulus:

$$\overline{E_0(s)} = \frac{\overline{\sigma(s)}}{\overline{\varepsilon(s)}} = (E_0 + \mu s) \tag{26}$$

Substituting of equation (23) with equation (26), and inversely transforming the Laplace to the time domain, leads to

$$P(t) = \frac{4\sqrt{R}E_0V^{3/2}}{3(1-\nu^2)}\left(t^{3/2} + \frac{3}{2}\tau t^{1/2}\right) \tag{27}$$

where $\tau = \mu/E_0$ is defined as the relaxation time [34].

Once τ was determined by fitting the force-time $P(t)$ curve with equation (27), equation (24) can be written into the form of

$$\sigma = E_0\varepsilon + \mu\frac{d\varepsilon}{dt} = E_0\varepsilon + E_0\tau\frac{d\varepsilon}{dt} \tag{28}$$

For simplicity, here we define an engineering strain $\bar{\varepsilon} \approx \frac{\bar{\delta}}{R}$, i.e., the ratio of a mean approach $\bar{\delta}$ to the effective radius R, and let $\varepsilon = \bar{\varepsilon}$; the equation (28) can be rearranged as

$$\sigma = E_0\bar{\varepsilon} + E_0\tau\frac{d(\frac{\bar{\delta}}{R})}{dt} = E_0\bar{\varepsilon}(1 + \tau\frac{V}{R\bar{\varepsilon}}) \tag{29}$$

Substituting equation (24) into equation (29), the $E(t)$ can be expressed as

$$E(t) = E_0 + E_0 \frac{\tau V}{R\bar{\varepsilon}} = E_0 \left(1 + \frac{\tau V}{\bar{\delta}}\right) \tag{30}$$

Therefore, the equation (30) provides a relationship between the Young's modulus and the separation speed V.

4. Results and Discussion

Figure 5 compares experimental measurements with the predictions of the JKR theory and shows consistency in the force-approach $P(\delta)$ curve for a constant unloading speed of 20μm/s. Using least-squares fitting the measured $P(\delta)$ curve with equation (6) and equation (7), the work of adhesion and the reduced Young's modulus of the spheres are determined to be $\Delta\gamma$ = (146±4) mN/m and E^* = (53±2) kPa, respectively. The Young's modulus is then calculated as E = (79±3) kPa if Poisson's ratio ν of the hydrogel spheres is assumed to be 0.5 (Cf. equation (3)). A comparable value of Young's modulus E = (72±3) kPa was measured from the spherical indentation test for the disk-shaped agarose sample by simply fitting with the loading force-indentation depth $F(h)$ curve with Hertz theoretical prediction, i.e. $F = \frac{4}{3}E^* R^{1/2} h^{3/2}$ (again, see Figure 4(b)). There was a liquid collar around the contact area, which manifest as a "negative" force in the force-indentation depth curve. However, liquid bridge force has no significant influence on the determination of the Young's modulus of the hydrogel, because the mechanical force dominant region (0.2-0.4 mN) of force-indentation depth curve was used in the analysis. Hyper-elastic behaviors often exhibit in soft matter such as hydrogel materials under large deformation. However, both the experimental curves of the pull-off $P(\delta)$ and indentation testing $F(h)$ do not manifest such non-linear behaviors because they were measured under small deformations (engineering strains <1.5%).

It is worth to note that the water surface tension γ_{LV} is ca. 72 mN/m at room temperature[28], which is consistent with the theoretical prediction of $\Delta\gamma = 2\gamma_{LV}$ (Cf. equation (16)). For the current case (R≈250 μm, r_m≈ −1 to −7 μm), μ_T^c was found to be in the range of 0.9 to 6.2. Since the values of μ_T^c are larger than 0.1, the DMT approximation is not applicable. Due to the lack of explicit solutions for the DMT-JKR transition, and only empirical equations being available[36], the JKR theory is the most suitable for fitting with the $P(\delta)$ curves.

Figure 5.

Figure 6.

Figure 6(a) shows the experimentally measured $P(\delta)$ curves for various separation speeds. The $P(\delta)$ curves for the higher speeds clearly show the increase in their slopes due to viscoelastic deformation. Fracture mechanics[37,38] shows that the contact line between two deformable solids can be considered as the crack tip of a crack path along the interface, and the work of adhesion Δγ is equal to the critical elastic energy release rate G, for crack initiation or propagation. Previous experiments for viscoelastic solids show the relationship $G(v,t) = G_0[1 + f(v,T)]$ between G, crack tip velocity v and temperature T[39–41]. G_0 is the threshold value when an arrested crack is about to grow. The factor $f(v,T)$ depends on the viscoelastic dissipation of the elastomers close to the cracktip, which increases with the increment of v. Thus, the work of adhesion between viscoelastic spheres in a dry contact is expected to increase with the separation speed. Figure 6(b) shows the JKR-fitted Δγ values for the current capillary adhesion to be independent of the separation speed in contrast to the dry-contact, while E exhibits a linear increase manifesting typical viscoelastic behavior of hydrogel materials. To examine the viscoelasticity of the spheres, Figure 7(a) shows least-squares fitting experimental force-time $P(t)$ curve at a speed 20μm/s with the equation (27) of the

viscoelastic model to determine the relaxation time $\tau = 0.17$ s, which demonstrates a considerable liquid-like behavior apart from their elastic deformation behavior[42]. Moreover, Figure 7(b) shows the comparison of the measured Young's modulus E at various separation speeds (also see Figure 6(b)) and the prediction of the viscoelastic model using the equation (30) for various separation speeds V=10-30 μm/s. Hence the viscoelastic model of section 3.2 provides a quantitative interpretation for the increase of the Young's modulus as separation speed increases.

Figure 7.

We also examined the roughness of the particle surfaces using an optical 3D microscope (Bruker, ContourGT-K). The Root Mean Square (RMS) roughness of surface was measured around 4.2μm. Several studies[43,44] have shown rubber-like materials with similar magnitudes of surface roughness under dry contact have noticeably lower adhesion values even at a much higher separation speed. Therefore, our results imply that the adhesion of the agarose particles is mainly originated from the water-vapor interfacial surface tension, which is less susceptible to the surface roughness and the separation speed. It is worth pointing out that the liquid bridge can be formed spontaneously between the particles subject to a compressive force, irrespective of their surface roughness and the ambient humidity. Although the two hydrogel spheres are viscoelastic, the structure of their contact region is regulated by the same physics that establishes the shapes of liquid droplets. A similar phenomenon in the adhesion occurred in the case of a rigid particle in contact with a soft gel substrate has been described by Jensen *et al.*[45]. For solids, the difference between surface free energy γand surface tension σis well distinguished. The surface free energy is defined as the work required to create a new unit of area reversibly and isothermally, while the surface tension is the amount of the reversible work per unit area needed to stretch a

pre-existing surface elastically. For liquids, the surface free energy and the surface tension are identical, while for solid materials, γ does not necessarily equal to σ.[46–48] Maugis suggested that for an ideal case of solids 1 and 2 forming a single crystal, the interfacial energy γ_{12} should be zero in the aforementioned Young-Dupré equation ($\Delta\gamma = \gamma_1 + \gamma_2 - \gamma_{12}$), and the energy $\Delta\gamma$ should equal 2γ, which is the cohesive energy[49]; referring to the capillary bridge between the two hydrogel particles in the current case. A corresponding physical mechanism exists in the solid-liquid interphase of the two hydrogel particles, in which liquid capillary bridges their contact. Because the liquid phase dominates the surface tension, the surface energy between the two agarose hydrogel particles should be identical to the surface tension of the solvent. This can be confirmed by our current experiment as $\Delta\gamma$ is equal to twice the surface tension of water γ_{LV}, which alludes to the physical interaction of two spherical liquid droplets. This interesting behavior may be attributed to the porous microstructure of agarose gel which retains typically water content more than 90% weight for weight.

5. Conclusions

We have directly measured the unloading $P(\delta)$ curves and the side-view profiles between two liquid-bridged agarose microspheres at various separation speeds. The JKR theory has been successfully applied to interpret the measured $P(\delta)$ curves of the microparticles for the quantitative estimation of their mechanical and interfacial properties. Our finding demonstrates that the hydrogel particles exhibit viscoelastic deformation under mechanical forces, while their interparticle adhesion is governed by the surface tension. Moreover, the work of adhesion shows to be independent of the separation speed and, by contrast, Young's modulus exhibits a linear increase that can be interpreted by the viscoelastic model proposed in section 3.2. Therefore mechanical characterization of capillary adhesion will be essential for the soft particulate materials

to improve material properties in their applications such as food processing and drug delivery.

CRediT author statement

Lidong Liu: Methodology, Software, Investigation, Data curation, Writing- Original draft preparation,

Kuo-Kang Liu: Supervision, Validation, Writing- Reviewing and Editing.

Declaration of interests

The authors declare that they have no known competing financial interests or personal relationships that could have appeared to influence the work reported in this paper

Acknowledgements

The authors thank Kai-Tak Wan (Northeastern University, USA) for helpful discussions, and Leverhulme Trust for support via Grant No. PRG-2012-738.

Appendix

Figure 1A.

REFERENCES:

[1] C.D. Willett, M.J. Adams, S.A. Johnson, J.P.K. Seville, Capillary bridges between two spherical bodies, Langmuir. 16 (2000) 9396–9405.

[2] M. Berhanu, A. Kudrolli, Heterogeneous structure of granular aggregates with capillary interactions, Phys. Rev. Lett. 105 (2010) 098002.

[3] L. Bocquet, E. Charlaix, S. Ciliberto, J. Crassous, Moisture-induced ageing in granular media and the kinetics of capillary condensation, Nature. 396 (1998) 735–737.

[4] Y.S. Chu, S. Dufour, J.P. Thiery, E. Perez, F. Pincet, Johnson-Kendall-Roberts theory applied to living cells, Phys. Rev. Lett. 94 (2005) 028102.

[5] J.P. Shelby, J. White, K. Ganesan, P.K. Rathod, D.T. Chiu, A microfluidic model for single-cell capillary obstruction by Plasmodium falciparum-infected erythrocytes, Proc. Natl. Acad. Sci. U. S. A. 100 (2003) 14618–14622.

[6] F. Zhao, D. Yao, R. Guo, L. Deng, A. Dong, J. Zhang, Composites of polymer hydrogels and nanoparticulate systems for biomedical and pharmaceutical applications, Nanomaterials. 5 (2015) 2054–2130.

[7] J.B. Sokoloff, Effects of capillary forces on a hydrogel sphere pressed against a surface, Langmuir. 32 (2016) 135–139.

[8] K. Farzanian, A. Ghahremaninezhad, The effect of the capillary forces on the desorption of hydrogels in contact with a porous cementitious material, Mater. Struct. 50 (2017) 216.

[9] K.L. Johnson, K. Kendall, A.D. Roberts, Surface energy and the contact of

elastic solids, Proc. R. Soc. London. A. Math. Phys. Sci. 324 (1971) 301–313.

[10] B.V. Derjaguin, V.M. Muller, Y.P. Toporov, Effect of contact deformation on the adhesion of elastic solids, J. Colloid Interface Sci. 53 (1975) 314–326.

[11] D. Maugis, B. Gauthier-Manuel, JKR-DMT transition in the presence of a liquid meniscus, J. Adhes. Sci. Technol. 8 (1994) 1311–1322.

[12] D. Maugis, Adhesion of spheres: The JKR-DMT transition using a Dugdale model, J. Colloid Interface Sci. 150 (1992) 243–269.

[13] S. Gupta, S.K. Kundu, J. Stellbrink, L. Willner, J. Allgaier, D. Richter, Advanced rheological characterization of soft colloidal model systems, J. Phys. Condens. Matter. 24 (2012) 464102.

[14] Y. Wang, X. Tang, G. Nian, Z. Suo, Strength and toughness of adhesion of soft materials measured in lap shear, J. Mech. Phys. Solids. 143 (2020) 103988.

[15] M.G. Mazza, The physics of biofilms - an introduction, J. Phys. D. Appl. Phys. 49 (2016) 203001.

[16] S. Leroch, M. Wendland, Influence of capillary bridge formation onto the silica nanoparticle interaction studied by grand canonical Monte Carlo simulations, Langmuir. 29 (2013) 12410–12420.

[17] X. Xu, A. Jagota, C.Y. Hui, Effects of surface tension on the adhesive contact of a rigid sphere to a compliant substrate, Soft Matter. 10 (2014) 4625–4632.

[18] X. Zhu, W. Xu, Effect of surface tension on the behavior of adhesive contact based on Lennard-Jones potential law, J. Mech. Phys. Solids. 111 (2018) 170–183.

[19] A. Ptak, H. Gojzewski, M. Kappl, H.J. Butt, Influence of humidity on the nanoadhesion between a hydrophobic and a hydrophilic surface, Chem. Phys. Lett. 503 (2011) 66–70.

[20] M. Farshchi-Tabrizia, M. Kappl, H.J. Butt, Influence of humidity on adhesion: An atomic force microscope study, J. Adhes. Sci. Technol. 22 (2008) 181–203.

[21] H.K. Christenson, J.N. Israelachvili, Growth of ionic crystallites on exposed surface, J. Colloid Interface Sci. 117 (1987) 576–577.

[22] P.J. Van Zwol, G. Palasantzas, J.T.M. De Hosson, Influence of roughness on capillary forces between hydrophilic surfaces, Phys. Rev. E. 78 (2008) 031606.

[23] B. Zhao, H. Zeng, Y. Tian, J. Israelachvili, Adhesion and detachment mechanisms of sugar surfaces from the solid(glassy) to liquid(viscous) states, Proc. Natl. Acad. Sci. U. S. A. 103 (2006) 19624–19629.

[24] H. Hertz, Ueber die Berührung fester elastischer Körper, J. Reine Angew. Math. 92 (1882) 156–171.

[25] S. Wu, Polymer interface and adhesion, M. Dekker, New York, 1982.

[26] D. Tabor, Surface forces and surface interactions, J. Colloid Interface Sci. 58 (1977) 2–13.

[27] R.L. Fisher, Direct measurement of the effect of meniscus forces on adhesion: a study of the applicability of macroscopic thermodynamics to microscopic liquid interfaces, Colloids Surf. 3 (1981) 303–319.

[28] A.W. Adamson, A.P. Gast, Physical chemistry of surfaces, Interscience publishers, New York, 1967.

[29] A. Fogden, L.R. White, Contact elasticity in the presence of capillary condensation I. The nonadhesive Hertz problem, J. Colloid Interface Sci. 138 (1990) 414–430.

[30] D. Xu, K.M. Liechti, K. Ravi-Chandar, On the modified Tabor parameter for the JKR-DMT transition in the presence of a liquid meniscus, J. Colloid Interface Sci. 315 (2007) 772–785.

[31] M. Ciavarella, J. Joe, A. Papangelo, J.R. Barber, The role of adhesion in contact mechanics, J. R. Soc. Interface. 16 (2019) 20180738.

[32] H. Yu, Z. Li, Q.J. Wang, Viscoelastic-adhesive contact modeling: Application to the characterization of the viscoelastic behavior of materials, Mech. Mater. 60 (2013) 55–65.

[33] X. Zhu, E. Siamantouras, K.K. Liu, X. Liu, Determination of work of adhesion of biological cell under AFM bead indentation, J. Mech. Behav. Biomed. Mater. 56 (2016) 77–86.

[34] Y.C. Fung, Biomechanics: Mechanical properties of living tissues, Springer-Verlag New York, 1993.

[35] E.H. Lee, J.R.M. Radok, The Contact Problem for Visooelastia Bodies, J. Appl. Mech. 27 (1960) 438–444.

[36] R.W. Carpick, D.F. Ogletree, M. Salmeron, A general equation for fitting contact area and friction vs load measurements, J. Colloid Interface Sci. 211 (1999) 395–400.

[37] J.A. Greenwood, K.L. Johnson, The mechanics of adhesion of viscoelastic

solids, Philos. Mag. A. 43 (1981) 697–711.

[38] K. Kendall, Cracks at adhesive interfaces, J. Adhes. Sci. Technol. 8 (1994) 1271–1284.

[39] B.N.J. Persson, E.A. Brener, Crack propagation in viscoelastic solids, Phys. Rev. E. 71 (2005) 036123.

[40] A.N. Gent, J. Schultz, Effect of wetting liquids on the strength of adhesion of viscoelastic materials, J. Adhes. 3 (1972) 281–294.

[41] D. Maugis, M. Barquins, Fracture mechanics and the adherence of viscoelastic bodies, J. Phys. D. Appl. Phys. 11 (1978) 1989–2023.

[42] M. Ahearne, Y. Yang, A.J. El Haj, K.Y. Then, K.K. Liu, Characterizing the viscoelastic properties of thin hydrogel-based constructs for tissue engineering applications, J. R. Soc. Interface. 2 (2005) 455–463.

[43] A. Tiwari, L. Dorogin, A.I. Bennett, K.D. Schulze, W.G. Sawyer, M. Tahir, G. Heinrich, B.N.J. Persson, The effect of surface roughness and viscoelasticity on rubber adhesion, Soft Matter. 13 (2017) 3602–3621.

[44] L. Dorogin, A. Tiwari, C. Rotella, P. Mangiagalli, B.N.J. Persson, Role of preload in adhesion of rough surfaces, Phys. Rev. Lett. 118 (2017) 238001.

[45] K.E. Jensen, R. Sarfati, R.W. Style, R. Boltyanskiy, A. Chakrabarti, M.K. Chaudhury, E.R. Dufresne, Wetting and phase separation in soft adhesion, Proc. Natl. Acad. Sci. U. S. A. 112 (2015) 14490–14494.

[46] R. Shuttleworth, The surface tension of solids, Proc. Phys. Soc. Sect. A. 63 (1950) 444.

[47] R.C. Cammarata, Surface and interface stress effects in thin films, Prog. Surf. Sci. 46 (1994) 1–38.

[48] E. Orowan, Surface energy and surface tension in solids and liquids, Proc. R. Soc. London. A. 316 (1970) 473–491.

[49] D. Maugis, Contact, adhesion and rupture of elastic solids, Springer Science & Business Media, 2013.

List of figure legends:

Figure 1. (a) Schematic (not to scale) and (b) image of the experimental setup to measure adhesion.

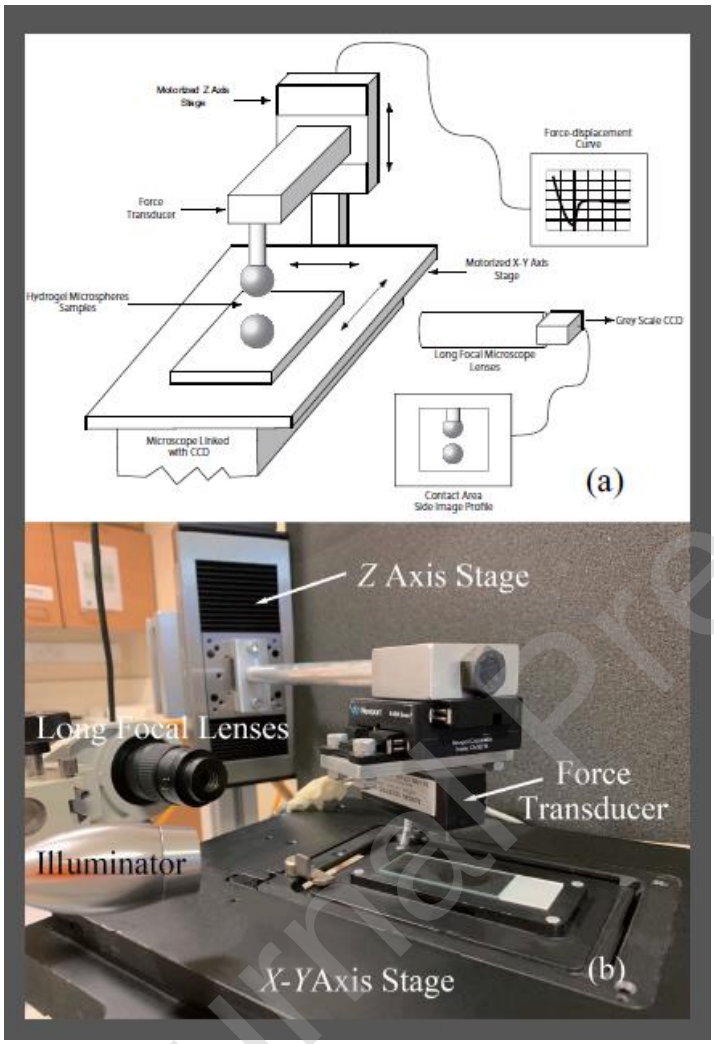

Figure 2. (a) Micrographs and (b) schematic of the liquid bridge formed between two

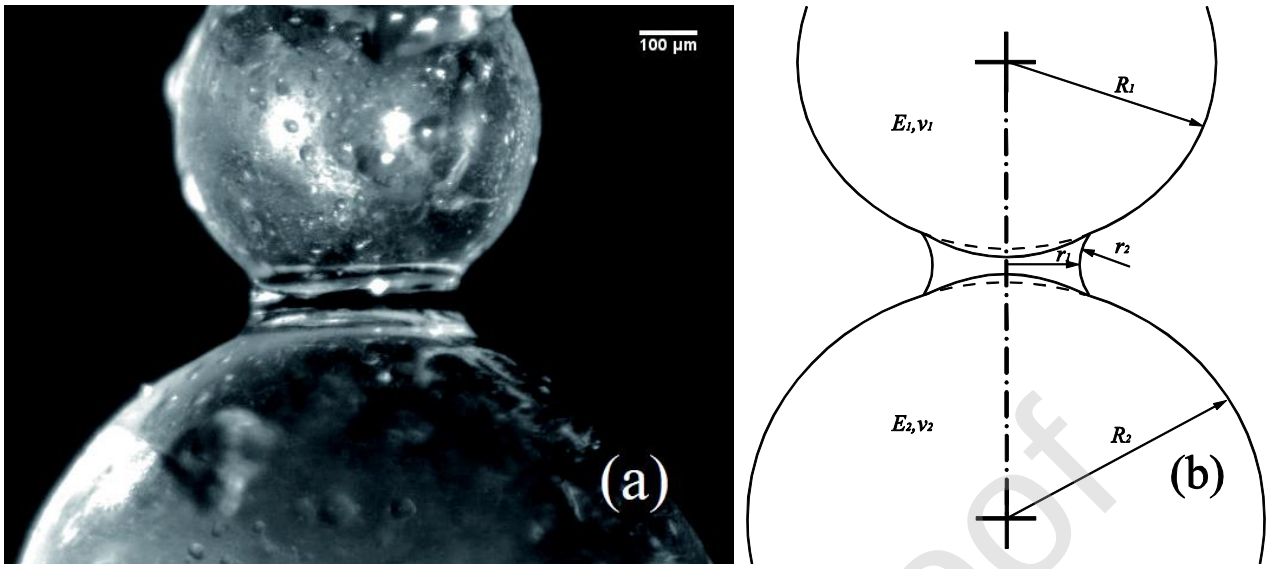

Figure 3. The side-view images acquired at a constant separation speed 20μm/s, show (a) the capillary breakage and (b) the liquid re-aborted completely after 0.166 sec.

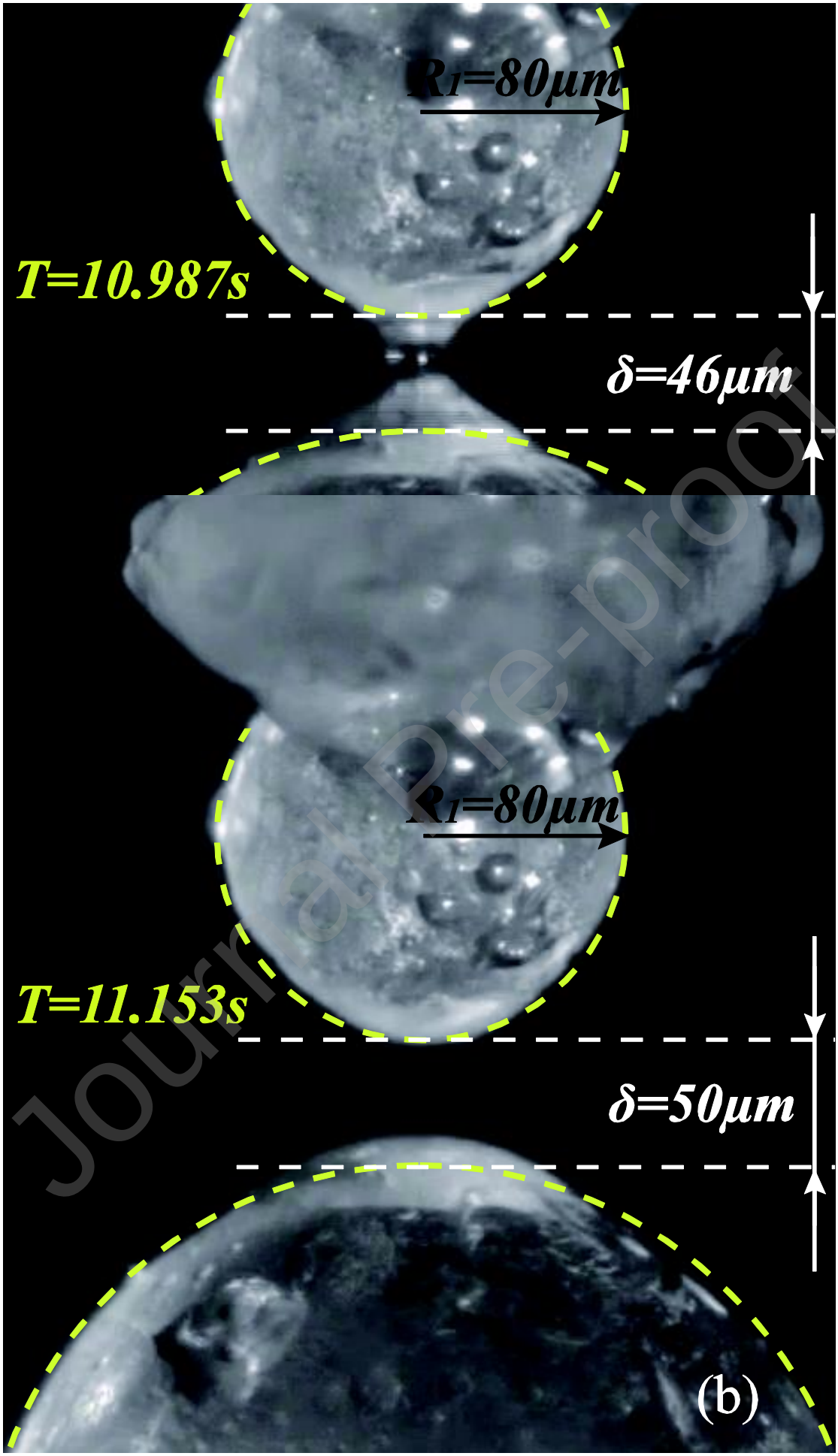

Figure 4. (a) Schematic of the alternative spherical indentation test for measuring Young's modulus of the agarose gel independently (not to scale). (b) Comparison of theoretical and the experimental indentation force F versus indentation depth h, $F(h)$ curve (measured at a constant loading speed 20μm/s). Young's modulus was 72 kPa for the prediction of Hertz theory with least-square fitting.

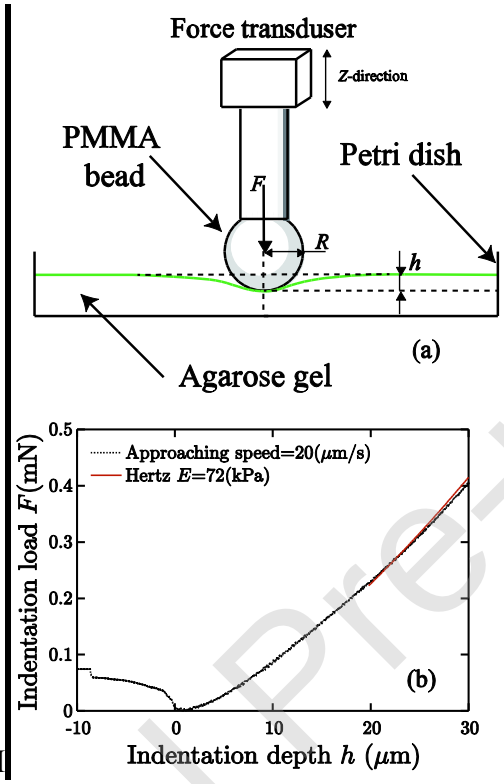

Figure 5. Comparison of experimental force-approach $P(\delta)$ curve (measured at a constant separation speed 20μm/s) and the JKR theoretical prediction with least-square

fitting.

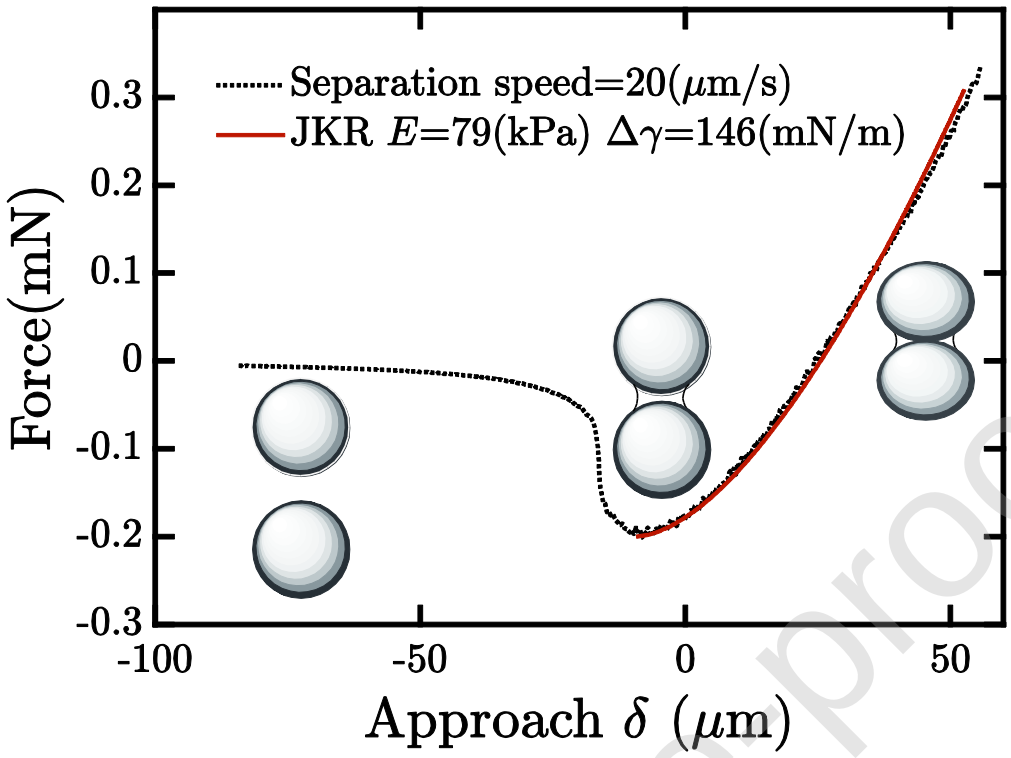

Figure 6. (a) The unloading force-approach $P(\delta)$ curves measured at different separation speeds. (b) The JKR-fitted values of Young's modulus E and work of adhesion $\Delta\gamma$.

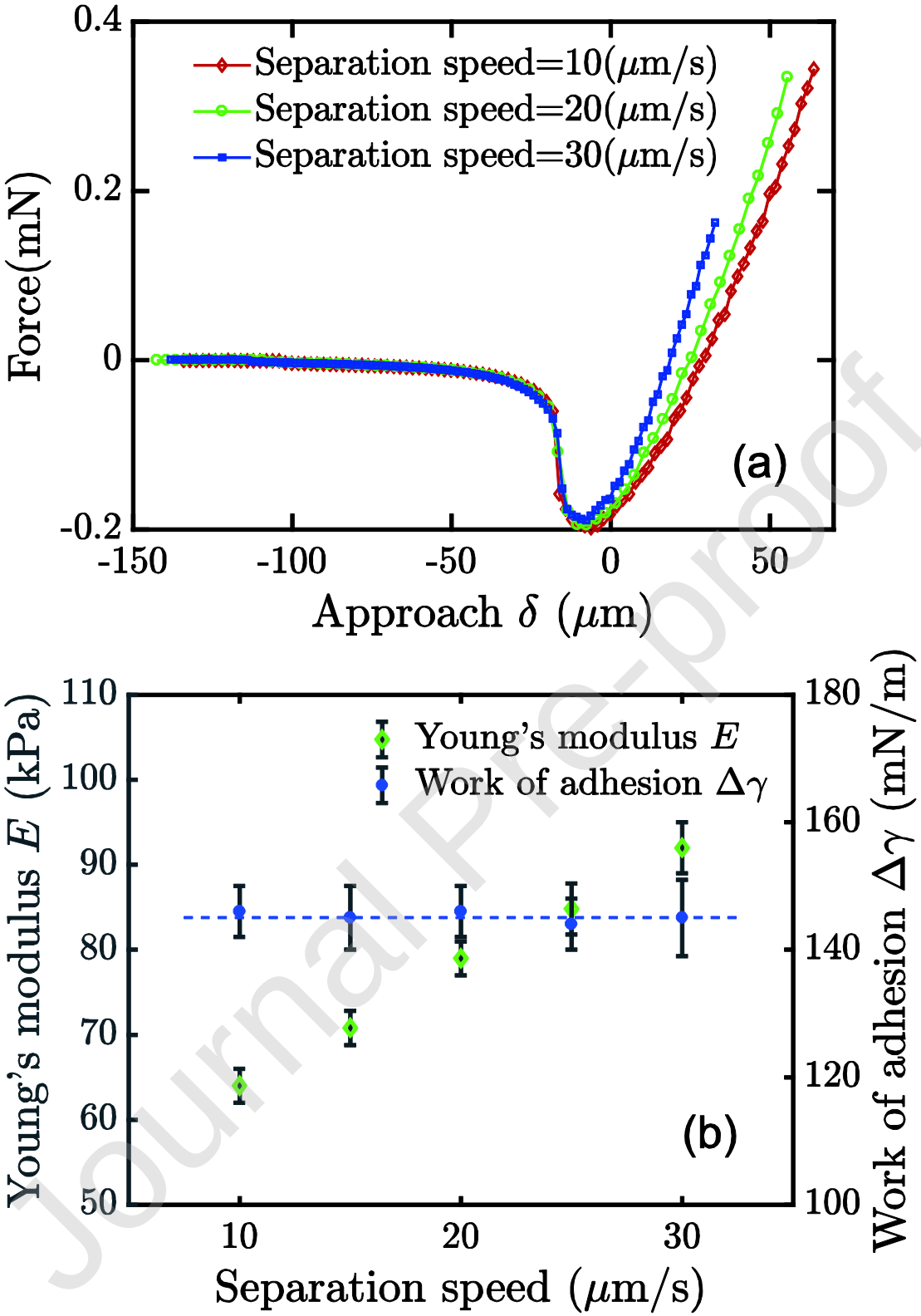

Figure 7. (a) Using least-squares fitting experimental force-time $P(t)$ curve (measured at a constant speed 20μm/s) with the equation (27). (b) Comparison of the measured Young's modulus E at various separation speeds and the prediction of the viscoelastic model using the equation (30).

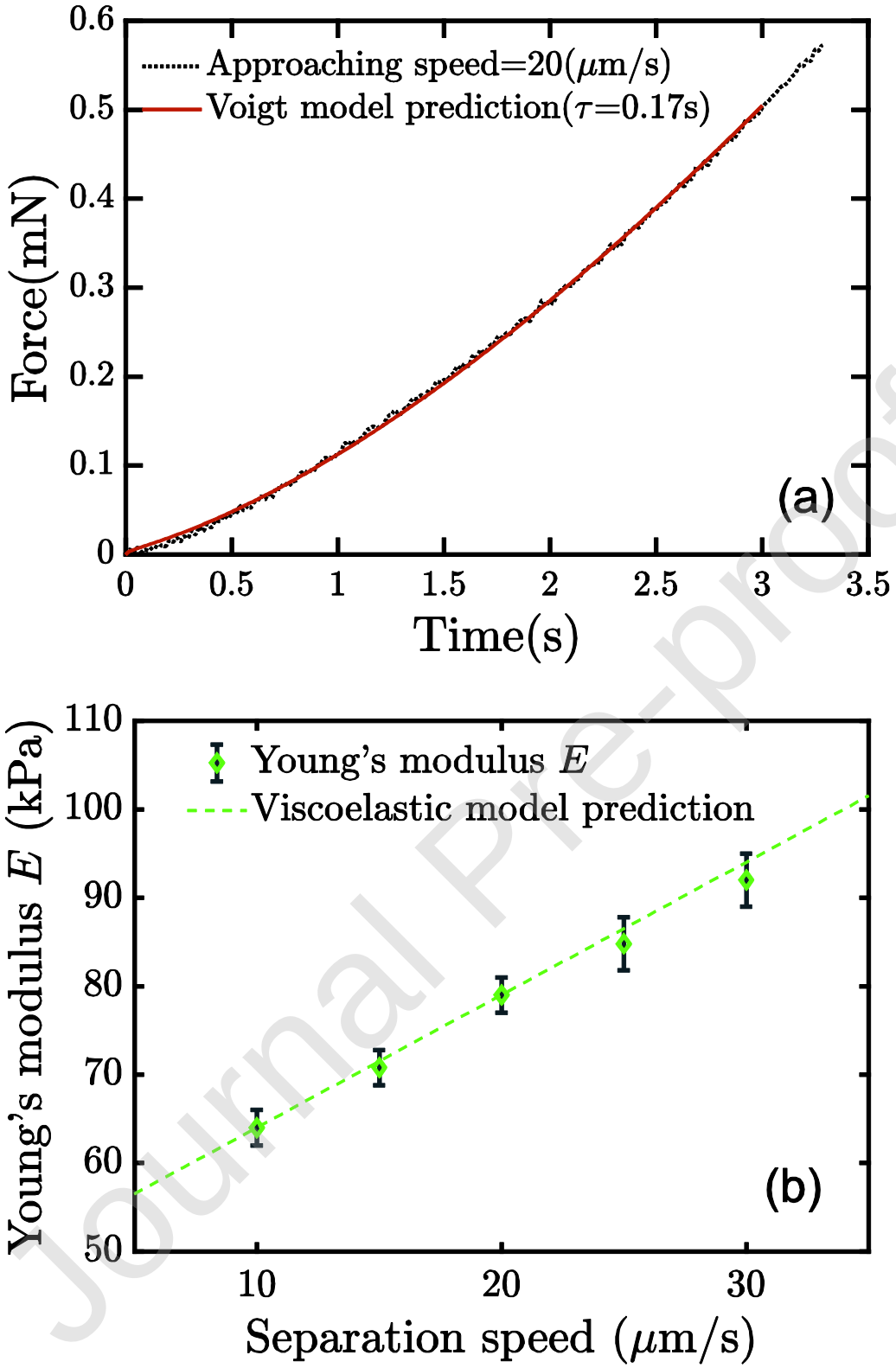

Figure 1A. Schematic diagram of Voigt model, the system consists of a Newtonian dashpot and linear elastic spring connected in parallel undergoing the same deformation.